Coastal Engineering 191 (2024) 104539

Contents lists available at ScienceDirect

Coastal Engineering

journal homepage: www.elsevier.com/locate/coastaleng

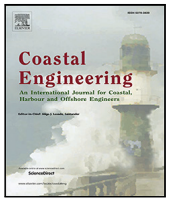

A physical model study on the hydraulic performances of vertical breakwaters with retreated wave walls

Alessandro Romano [a,b,*], Matteo Centorami [a], Claudia Cecioni [a], Giorgio Bellotti [a]

[a] Roma Tre University, Department of Civil, Computer Science and Aeronautical Technologies Engineering, Rome 00146, Italy
[b] IHCantabria - Instituto de Hidráulica Ambiental de la Universidad de Cantabria, Calle Isabel Torres 15, Santander 39011, Spain

ARTICLE INFO

Keywords:
Vertical breakwaters
Retreated wall
Wave-structure interaction
Physical model tests
Water waves

ABSTRACT

This paper describes a 2D physical model study on the hydraulic performances of composite vertical breakwaters with retreated wave walls. The research is an expansion of a previous experimental study by the same Authors: a very large number of experiments, in the order of 2,000, have been carried out by exploring and varying a wide range of wave and geometrical parameters of the structure, to investigate their effect and importance. In order to make feasible the execution of this large number of tests, a small-scale wave flume was used and regular wave conditions were reproduced. The influence of the wave wall retreat has been investigated in terms of wave-induced forces, reflection coefficients and wave overtopping discharges, comparing the hydraulic performances of structures with retreated walls with those of a flushed wall configuration under the same wave conditions. The large number of experiments allowed to formulate a detailed description of the complex phenomena at hand, providing statistical indicators that can be used as guidelines for preliminary design purposes of such structures, quantifying the relevant sources of uncertainty. The analysis confirmed and extended the previous findings and indicates that, on average, the hydraulic performances of structures with retreated crown wall vary significantly from those of flushed wall configurations. Specifically: (I) the forces acting on the wave wall increase of a factor up to 1.5, due to the occurrence of impulsive loads; (II) the forces acting on the caisson trunk decrease of a factor up to 0.91; (III) the global forces can decrease reaching a minimum reduction factor of 0.87, although some dangerous exceptions, in which equal or larger loads, than those occurring for standard flushed wall configuration, have been registered; (IV) the reflection coefficients decrease of a factor up to 0.83; (V) the wave overtopping discharges increase up to 2.55 times those with flushed walls.

1. Introduction

Vertical breakwaters are monolithic structures often used to protect harbour basins. They are composed of (i) a rubble mound foundation, (ii) a precast concrete trunk, (iii) a superstructure cast in situ, (iv) a wave wall. Typically, the front faces of the trunk and of the wave wall are aligned, offering a vertical and smooth surface at which wave reflection takes place, inducing a pulsating wave load on the whole structure. A technical solution for trying to reduce the wave loads on the breakwater, consists in placing the wave wall at a retreated position with respect to the front face of the trunk. This is expected to favor a time shifting between the wave loads acting on the trunk and those acting on the wave wall, reducing the global instantaneous peak forces.

However, no design criteria or guidelines exist to assist engineers in the implementation of such technique. In fact, most of the available literature (Goda, 2010; Takahashi, 1996; Oumeraci et al., 2001; Martinelli and Lamberti, 2011) concentrates on flushed wave wall structures, while several works addressed the study of wave loads induced by breaking waves on vertical walls placed in shallow water conditions (Cooker and Peregrine, 1990; Bullock et al., 2007; Bredmose et al., 2009; Cuomo et al., 2010a,b; Bredmose et al., 2015). Indeed, studies that investigate forces and pressures on retreated walls placed on tops of smooth dikes and rubble mound breakwaters are available (e.g., Martin et al., 1999; van Gent, 2003; De Rouck et al., 2012; Chen et al., 2015; Van Doorslaer et al., 2017; Molines et al., 2019; De Finis et al., 2020; Cao et al., 2021; Chen et al., 2021), but the physical processes that take place at this type of structures appear to be significantly different from those for vertical walls.

In order to make a step forward in the understanding of the physical processes and of the governing factors, which might play a role in the reduction of the wave loads on such specific type of structures, a series

* Corresponding author at: Roma Tre University, Department of Civil, Computer Science and Aeronautical Technologies Engineering, Rome 00146, Italy.
E-mail address: alessandro.romano@uniroma3.it (A. Romano).

https://doi.org/10.1016/j.coastaleng.2024.104539
Received 11 April 2024; Received in revised form 9 May 2024; Accepted 12 May 2024
Available online 14 May 2024

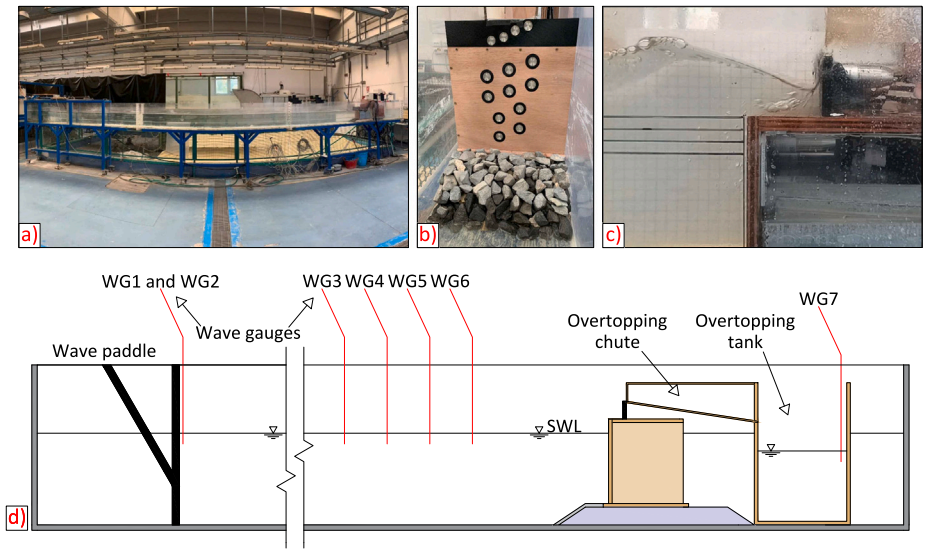

Fig. 1. Panel (a): picture (lateral view) of the wave flume. Panel (b): picture (front view) of the caisson model (trunk in marine plywood and 3D printed wave wall) with pressure sensors. Panel (c): picture (lateral view) of the wave wall during an impact. Panel (d): sketch of the wave flume, model structure and overtopping chute and tank.

of experimental investigations was recently undertaken by the Authors. The first results have been published in a previous paper (Romano and Bellotti, 2023), which reports the results of an experimental campaign carried out in a wave flume and describes the basic phenomena involved and the physical/geometrical drivers expected to play a role on the force increase/reduction factor. The geometry of the caisson and of the rubble mound foundation was kept constant and four wave wall positions (one aligned with the trunk and three retreated) had been reproduced. Moreover, the wave wall had been designed, on purpose, high enough to avoid the wave overtopping. The experiments had been carried out using 19 regular wave conditions for each geometry, resulting in a total of 76 tests.

Despite the limited number of geometries and wave conditions, the experimental campaign by Romano and Bellotti (2023) has lead to a better understanding of the effects of the retreated wall and to identify the physical/geometrical drivers and preliminary conclusions/considerations, as follows:

- in general, the wave forces on the whole structure and on the caisson trunk tend to decrease as the wave wall retreat increases;
- the wave forces on the wall in general increase for retreated wall configurations;
- the retreated wall is subject to impulsive loads, due to the development of a bore on the flat superstructure between the seaward edge of the trunk and the wave wall;
- the time shifting between wave loads on the trunk and impacts on the wall is significant only if the retreat of the wall is relevant. While small retreats induce to negligible shifting and strong impacts on the wall, resulting in equal or even larger global forces on the structure as a whole;
- a major source of wave loads reduction is given by the fact that reflection is reduced by the wave overtopping occurring at the seaside edge of the trunk, resulting in smaller wave pressures acting on the vertical front of the caisson;
- the physical processes mentioned above (impacts, time shifting, reduction of pressures at the seaside edge of the trunk) can have both a concordant and antithetical effect among them.

It was indeed clear that the physical processes that take place during the wave-structure interaction are quite complicated and deserve further investigation for better understanding. Also, the main drivers that play a role in the reduction of the global forces on the caisson, have been clearly identified in the previous research, but a very limited number of combinations of the geometry and wave parameters have been tested. Thus, these first insights have motivated an expansion of the previous experimental campaign, which is described in the present paper.

The main aim of the new campaign is twofold: (1) to expand the database of forces, reflection coefficients and overtopping rate acting on vertical breakwaters with flushed and retreated wave walls and (2) to make insight on the influence of the retreated wall distance on the hydraulic performances of such structures. Thus, in the new campaign, the range of tested wave and geometrical parameters of the structure (e.g., more different positions of the wave wall, water depths, heights of the rubble mound foundation, etc.) has been expanded, by performing a very large number of experiments, in order to investigate their effect and importance. Therefore, these parameters ranges have been systematically varied to make sure that a broad set of wave-structure interaction conditions are modeled and explored. Moreover, wave overtopping is measured for each test, as it is one fundamental hydraulic performance parameter that was not considered in Romano and Bellotti (2023). In order to make feasible the execution of a very large number of tests (about 2,000), a small-scale wave flume was used and regular wave conditions were reproduced. These choices of course might represent a limitation of the present results, that is discussed in detail later in the paper, but appear to be a reasonable approach to understand the complex physical processes at hand (Ravindar et al., 2021).

The paper is structured as follows. After this introduction, a description of the experimental setup, together with the model structure and the wave conditions, is provided. Then, a detailed description and discussion of the experimental results, together with the limitations of the present study, is given. Finally, conclusions and ongoing research close the paper.

2. Experimental setup

2.1. Wave flume

The new 2D experiments have been performed in the hydraulics laboratory of Roma Tre University (Department of Civil, Computer Science and Aeronautical Technologies Engineering, Rome, Italy). The laboratory is equipped with a small-scale wave flume made of Perspex, pictured in panel (a) of Fig. 1. The flume is 9.00 m long, 0.27 m wide and 0.50 m high, and has a piston-type wave maker with a maximum

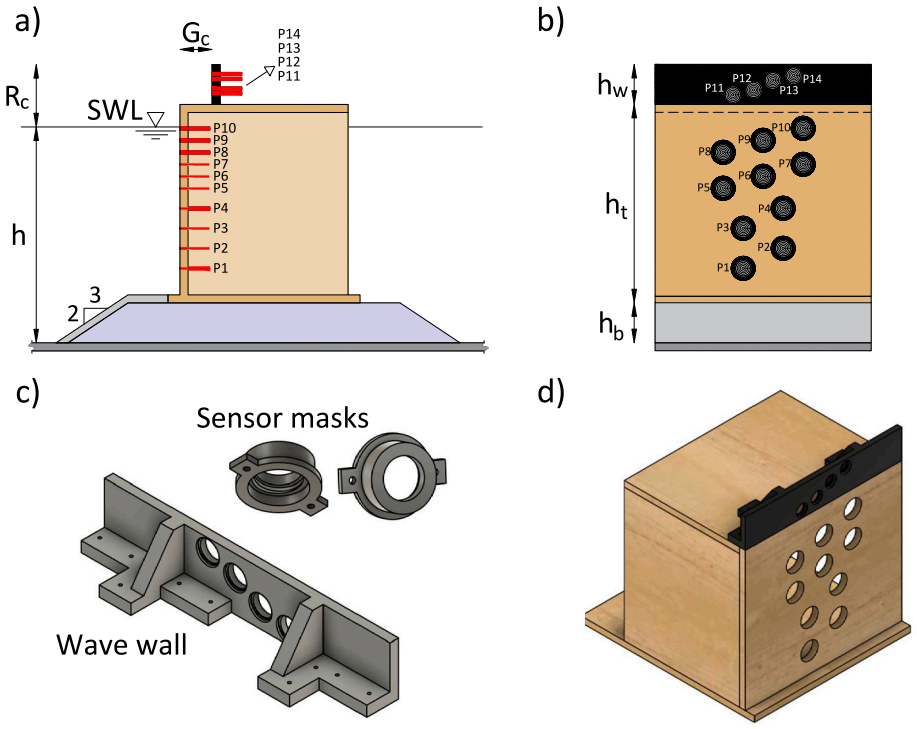

Fig. 2. Panel (a) and (b): sketch of the pressure sensor positions and geometrical parameters. Panel (c): detail of the 3D printed wave wall and pressure masks with thread. Panel (d): 3D render of the model structure with wave wall and pressure sensors housing.

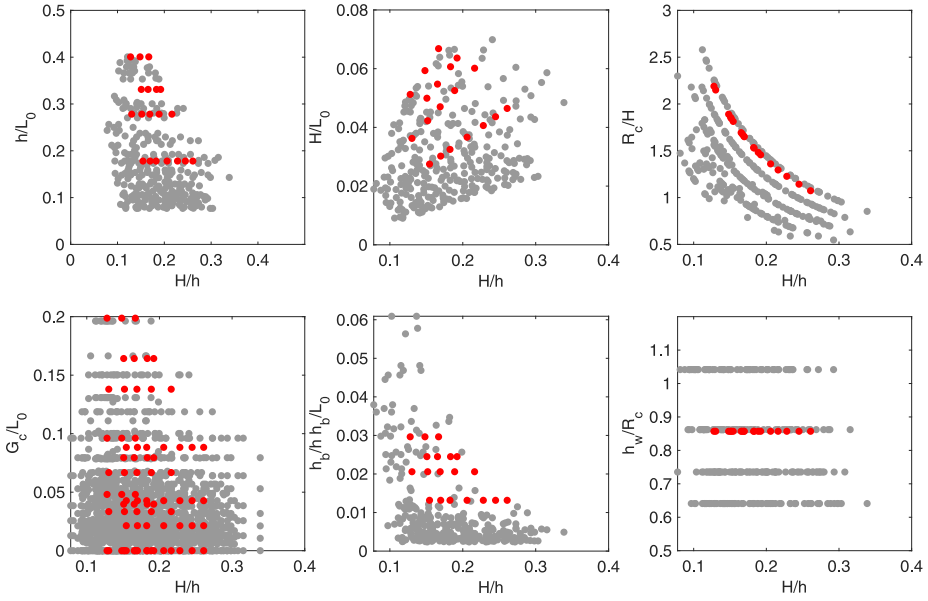

Fig. 3. Ranges of explored parameters tested during the new experimental campaign (filled gray dots). Note that filled red dots refer to the previous data of Romano and Bellotti (2023).

stroke of 1.00 m, allowing the generation of both regular and irregular waves. The wave generation system is controlled by the state of the art software AWASYS 7 (Aalborg University, 2018), that includes an active wave absorption system (Andersen et al., 2016, 2018).

A total of seven resistive wave gauges are positioned along the flume to measure the free surface elevation. As can be noted in the sketch of Fig. 1 (panel (d)), two wave gauges are fixed on the wave maker in order to provide the feedback to the active absorption system (WG1 and WG2). Four wave gauges have been aligned along the central longitudinal axis of the flume, to measure the wave field in front of the structure (WG3–WG6). The last wave gauge (WG7) is used to measure wave overtopping: it is placed in a fixed tank located behind the structure, in which the overtopping water volumes are collected through a chute. The acquisition frequency of the wave gauges is set at 50 Hz, and a calibration procedure is carried out at least twice daily to account for environmental variations.

2.2. Physical model

The model structure replicates a vertical breakwater placed on top of a rubble mound foundation (see Fig. 1, panel (b)). The foundation is made of two parts: an inner core of uniform-size rock material and an

Table 1
Pressure sensor names (first column), vertical positions measured from the toe of the caisson (second column) and areas of influence (third column). Note: areas are expressed in m as it is a 2D experiment.

Pressure sensor	Elevation (m)	Influence area (m)
$P1$	0.043	0.0455
$P2$	0.068	0.0250
$P3$	0.093	0.0250
$P4$	0.118	0.0250
$P5$	0.143	0.0250
$P6$	0.158	0.0150
$P7$	0.173	0.0150
$P8$	0.188	0.0150
$P9$	0.203	0.0150
$P10$	0.218	0.0375
$P11$	0.260	0.0150
$P12$	0.266	0.0090
$P13$	0.278	0.0090
$P14$	0.284	0.0170

external rubble mound layer made of rocks (weight range 10.0–20.0 g). The vertical breakwater is composed by the trunk, made of marine plywood (thickness 0.01 m) and the wave wall, made of plastic and designed to be fixed at different positions in order to test different wave wall retreats. In panel (c) of Fig. 1 the picture captures a wave impact on the wall during a test with retreated wall position. The caisson trunk height is $h_t = 0.248$ m and the wave wall height is $h_w = 0.050$ m; their width is 0.270 m to perfectly fit inside the wave flume. The dimensions of both the caisson trunk and the wall are kept constant during all the tests. The physical model is designed to be representative, in Froude similarity, of a quite broad range of vertical breakwater configurations in relatively deep-waters, rather than replicating a specific existing structure. Nevertheless, a scale factor of approximately 1:100 can be assumed, to get at prototype scales a composite vertical breakwater based on water depths in the range of 27.0–35.0 m, with freeboard values between 5.0–8.0 m. With this scale factor, considering also the other geometrical parameters, the tested structures refer to a typical Italian vertical breakwater (Franco, 1994).

To accurately measure the wave-induced actions on the vertical structure, 14 pressure transducers (P_i, $i = 1, 2, \ldots, 14$; TRAFAG Submersible Pressure Transmitter NAL 8838, with pressure range of 0–200 mbar) are fixed at the seaside face of the structure. The acquisition frequency of these pressure sensors is 7,000 Hz to effectively measure impulsive load peaks. As illustrated in Fig. 2 (panels (a) and (b)) and as can be noted in the model picture (Fig. 1, panel (b)), 10 sensors (P1–P10) are placed on the caisson trunk and 4 (P11–P14) on the wave wall. These transducers are strategically positioned in order to provide a very high spatial resolution. Moreover, to maximize the number of sensors in the areas of most interest, i.e. on the wave wall and around the mean sea level, the mutual distance between the pressure sensors is not constant, spanning in the range 0.006 m–0.025 m. In Table 1 pressure sensor names and positions are reported.

Due to the reduced scale of the experiments, a particular care has been adopted in minimizing potential laboratory effects. To this end, some special pieces have been ad-hoc designed and 3D-printed for housing the pressure sensors with the highest possible precision and minimizing possible sources of flow disturbance. In particular, the wave wall has been 3D-printed with plastic material, guaranteeing a structure as rigid as possible and equipped with threaded holes ready to house the pressure sensors (Fig. 2, panel (c)). On the other hand, to equip the caisson trunk with a large number of pressure sensors, and to ensure that its seaside face was as rigid and flat as possible, some special threaded masks for screwing the pressure sensors have been designed and 3D-printed (Fig. 2, panel (c)). These elements are fixed at the seaside face of the trunk, ensuring a very good alignment between themselves and the vertical caisson. Panel (d) of Fig. 2 shows a render of the model structure with the wave wall in the flushed configuration and the trunk ready for housing the sensor masks.

Table 2
Ranges of explored parameters tested during the new experimental campaign.

Parameters	Min. value	Max. value
H (m)	0.027	0.115
T (s)	0.700	1.630
h (m)	0.270	0.350
H/h (–)	0.090	0.373
h/L_0 (–)	0.077	0.393
H/L_0 (–)	0.008	0.077
R_c/H (–)	0.547	2.805
G_c/L_0 (–)	0.000	0.196
h_b/h (–)	0.167	0.313
h_w/R_c (–)	0.641	1.042

2.3. Test program

Fig. 3 presents the parameters space, showing the value of the main geometrical and wave parameters tested in the present experimental campaign (gray markers), together with those explored by Romano and Bellotti (2023) (red markers). All the panels of Fig. 3 use non-dimensional parameters axes, considering that h is the water depth at the toe of the rubble mound foundation; L_0 is the wave length in deep water conditions calculated as $L_0 = \frac{gT^2}{2\pi}$; H is the incident regular wave height; R_c is the crest wall freeboard; G_c is the horizontal wall retreat with respect to the seaward caisson face; h_b is the height of the rubble-mound foundation and h_w is the wall height (for geometrical parameters refer to Fig. 2 and List of Symbols).

The program for the new test campaign was thought in order to widen the range of the parameter values explored in the previous study (red markers in Fig. 3). Specifically, regarding the geometrical parameters, the experiments considered two different rubble mound foundation heights, $h_b = 0.05$ and 0.1 m; six different wave wall retreated positions: G_{c0} for the flushed wall configuration ($G_c = 0$) and G_{c1}–G_{c5}, respectively for $G_c = 0.00$, 0.02, 0.04, 0.06, 0.10 and 0.15 m. The wave wall height h_w is fixed, however the R_c value varies due to different water depth tested. The wave height and the wave period of the regular waves and the water depth are systematically varied within the following ranges: $0.027 \leq H \leq 0.115$ m, $0.7 \leq T \leq 1.63$ s, and $0.27 \leq h \leq 0.35$ m. Table 2 reports the range of tested parameters values.

Therefore, 322 wave and geometrical parameters combinations have been tested for each wall configuration, resulting in a total number of 1932 experiments, and allowing the comparison between the performances of the structure under the same wave conditions for the flushed wall configuration (G_{c0}) and for each wall retreat (from G_{c1} to G_{c5}). The duration of each test is approximately 75.0 s in order to obtain a wave time series long enough to get stationary conditions acting on the structure.

3. Results and discussion

In this section the experimental results are presented and discussed. The analysis is divided into three parts: (1) the analysis of the forces acting on the structure; (2) the analysis of the reflection coefficients; (3) the analysis of the wave overtopping. The last subsection discusses the limitations of the study.

3.1. Wave forces

For each experiment fourteen pressure signals have been analyzed in a time window of duration of 20.0 s, at which stationary conditions had already developed, avoiding the initial stages of each test. The pressure signals have been integrated by means of the rectangular integral method, assuming a uniform pressure along the area of influence of each sensor (see values in Table 1). The boundaries of the area of influence are at half the distance between the considered sensor and those above and below. Thus, the following quantities are obtained:

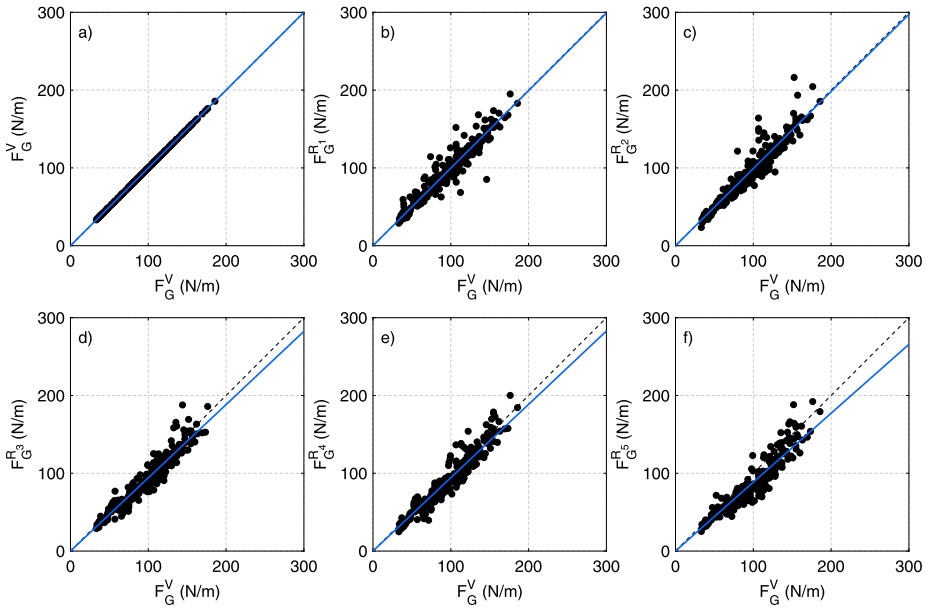

Fig. 4. Scatter plots of the global forces (filled black markers). In the panels from (b) (referring to G_{c1}) to (f) (referring to G_{c5}), $F_G^{R_i}$ are plotted against F_G^V, while in the panel (a) the same quantities (F_G^V, referring to G_{c0}) are reported in both the x- and y-axes. Note: the dashed black and continuous blue lines identify the bisector and trend lines, respectively.

the global force $F_G(t)$ (acting on the whole structure), the force acting on the caisson trunk $F_T(t)$, and the force acting on the wall $F_W(t)$ signals. No filtering has been used. The force peaks within the above mentioned time window have been identified and extracted. Thus, for each experiment, and for each considered force signal, a sample of force peaks is obtained. Since regular waves have been tested, average values of these peaks over the time window (hereinafter F_G, F_T, and F_W, which are the average global, trunk, and wall forces, respectively) are considered in the following analysis and discussion.

To identify the average peak forces related to the 6 positions of the wave wall, the following symbols are used throughout the paper: F_G^V, F_T^V, F_W^V, $F_G^{R_i}$, $F_T^{R_i}$, $F_W^{R_i}$ (see List of Symbols). Note that the apex $(\cdot)^V$, standing for "vertical", is used from now on throughout the whole manuscript to identify quantities related to the flushed wall configuration (G_{c0}). The apex $(\cdot)^{R_i}$ ($i = 1, \ldots, 5$) standing for "retreated", is used to identify quantities related to the five retreated wall configurations (G_{c1}–G_{c5}).

The analysis of the global forces is presented in Fig. 4. This figure is divided into six panels, distributed in two rows and three columns. In each panel, the experimental data are represented as filled black markers and are presented in the form of scatter plot, while the dashed black line identifies the bisector line. In the panels from (b) (referring to G_{c1}) to (f) (referring to G_{c5}), $F_G^{R_i}$ is plotted against F_G^V. Conversely, in the panel (a) the same quantities (F_G^V, referring to G_{c0}) are reported in both the x- and y-axes and of course perfectly align along the bisector line.

Thus, Fig. 4 provides a direct comparison in terms of global force increase/reduction as a function of the wave wall position, within the ranges of wave and structural parameters explored during the experiments. In order to help the interpretation of the results as well as to better understand the following analysis and considerations, the best fitting lines (in blue) are also represented in each panel. It is worth noticing that these fitting lines should not be intended as an empirical prediction method, in fact no correlation coefficients are reported. Instead, they just aim at providing an indication of the general trend/behavior for the considered wall retreat configuration. Conversely, in order to provide a quantitative estimate of the force increase/reduction factor as a function of the wall retreat to be used for engineering design, a statistical analysis is provided later in the section.

For small wall retreats (panels (b) and (c)) of Fig. 4, the data cloud lies preeminently along the bisector, although exhibiting a moderate dispersion that testifies the complex nature of the phenomena at hand. Therefore, the global forces acting on caissons with retreated wave wall are similar, sometimes larger, than those acting on caissons with flushed wall under the same wave conditions. As far as larger wall retreats are concerned (panels (d), (e) and (f)), the data cloud tends to lay, on average, at the right of the bisector lines, as also suggested by the fitting lines. Thus, the global forces acting on caissons with retreated wave walls tend to decrease with increasing G_c. Moreover, the rate of global force decrease tends to be larger when the wall is more retreated. These findings are consistent with those reported by Romano and Bellotti (2023). Nevertheless, it is interesting to note that, there exist conditions in which global forces acting on caissons with retreated crown walls are even larger than those experienced for the flushed wall configuration (under the same wave conditions) also for large wall retreats. This aspect testifies, one more time, the complex nature of the phenomena at hand and the complex interaction between the governing drivers. Therefore, due to the large number of data available and the complex mechanisms, a statistical approach based on statistical descriptors/indicators is used to quantify the force increase/reduction factor. This is discussed later in the section, after the description of the trunk and wall forces, respectively.

In Fig. 5 the analysis of the forces acting exclusively on the trunk is presented. The organization of this figure is exactly the same of Fig. 4, but here the trunk forces (F_T^V and $F_T^{R_i}$) are represented. These exhibit a behavior similar to that of the global forces (see Fig. 4). In fact, for small wall retreats (panels (b) and (c)), the data cloud is, on average, mainly aligned along the bisector, yet exhibiting a smaller dispersion if compared with the global forces. This is perfectly justified by the fact that the global forces also take into account the impacts on the wall, which can be characterized by impulsiveness also for small wall retreats. Similarly to what seen for global forces, for increasing values of wave wall retreats (panels (d), (e) and (f)) the data cloud tends to move, on average, on the right of the bisector lines. Again, this behavior is similar to that observed for the global forces (see Fig. 4) and it is consistent with the previous experimental findings of Romano and Bellotti (2023). Also the forces acting on the caisson trunk are treated later by means of a statistical analysis.

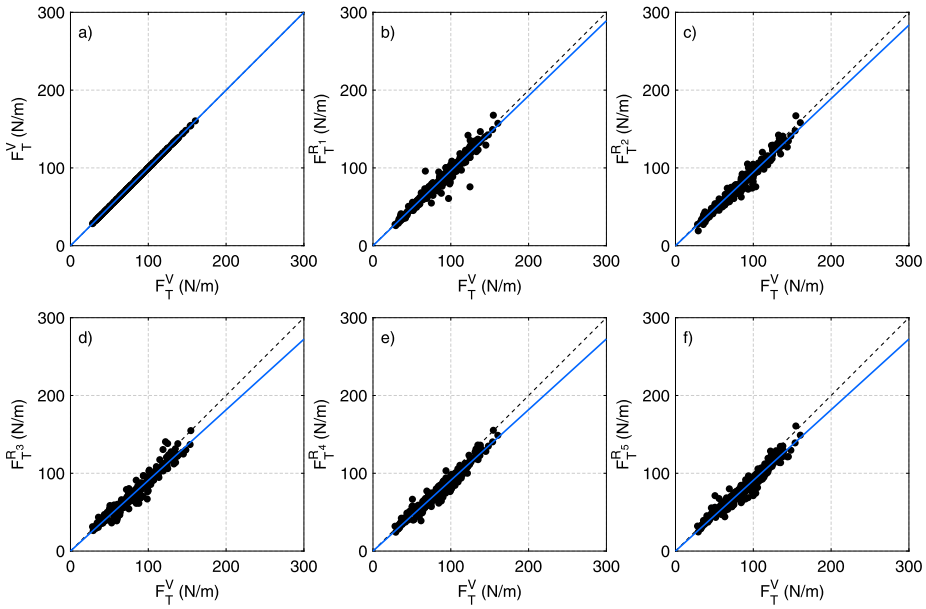

Fig. 5. Scatter plots of the trunk forces (filled black markers). In the panels from (b) (referring to G_{c1}) to (f) (referring to G_{c5}), $F_T^{R_i}$ are plotted against F_T^V, while in the panel (a) the same quantities (F_T^V, referring to G_{c0}) are reported in both the x- and y-axes. Note: the dashed black and continuous blue lines identify the bisector and trend lines, respectively.

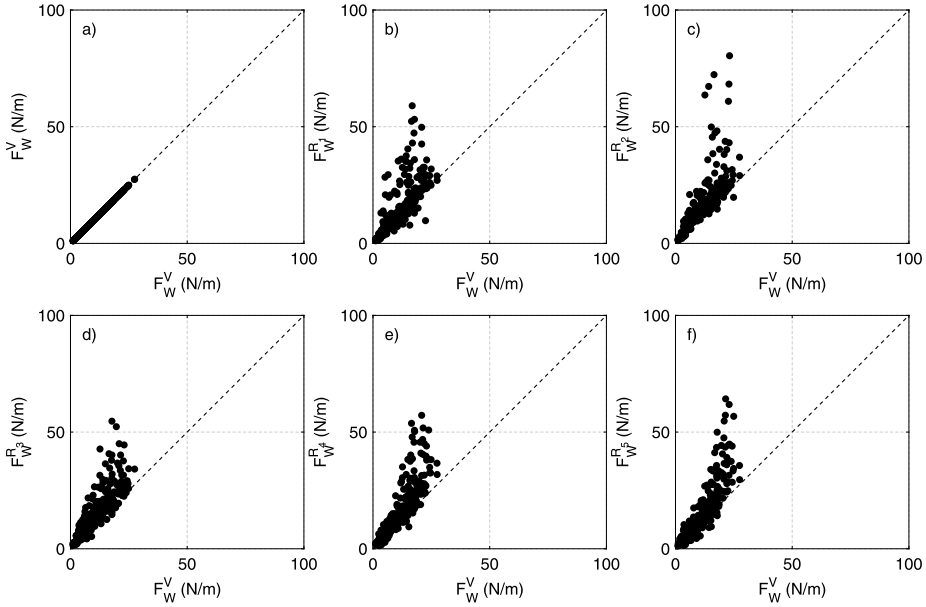

Fig. 6. Scatter plots of the wall forces (filled black markers). In the panels from (b) (referring to G_{c1}) to (f) (referring to G_{c5}), $F_W^{R_i}$ are plotted against F_W^V, while in the panel (a) the same quantities (F_W^V, referring to G_{c0}) are reported in both the x- and y-axes. Note: the dashed black line identifies the bisector line.

The Fig. 6 reports the analysis of the forces acting on the wave wall (F_W^V and $F_W^{R_i}$), using the same style of the previous figures. Here, however, the best fitting lines are not represented. In general, the behavior of the forces acting on the wall is very similar among all the wall retreat configurations tested. In fact, even for small wall retreats (panels (b) and (c)) the increase of the force acting on the crown wall is significant and the experimental data are characterized by a noticeable dispersion if compared with both the global and the trunk forces. This is, again, in line with the previous findings of Romano and Bellotti (2023), who pointed out that the increase on the wave loads acting on the wall, is mainly related to the change of flow regime induced by the retreated wall configuration, which leads to the occurrence of impulsive "church-roof-like" impacts, on the wall itself. For the same reason, this data dispersion is considered natural for such a phenomenon, considering that the forces acting on the wave wall are governed by the occurrence of impulsive impacts that have a short duration in time and a high variability in space. Moreover, as better explained later, it appears that, on average, the force increase on the wall does not increase significantly for increasing G_c. Statistical analysis of the data is presented later.

All the data represented in the Figs. 4, 5, and 6 have been further processed as follows: for each force component (global, trunk and wall) the ratios between the considered quantity measured for all the retreated wall configurations ($F_G^{R_i}$, $F_T^{R_i}$ and $F_W^{R_i}$) and those for the flushed wall configuration (F_G^V, F_T^V and F_W^V), obtained for the same wave conditions and structural parameters, have been calculated. Then, some statistical descriptors and indicators (i.e., mean, median,

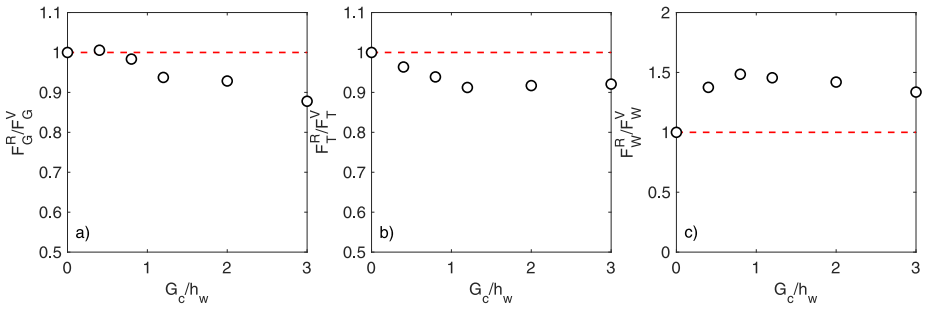

Fig. 7. Average values (empty black markers) of the ratios F_G^R/F_G^V, F_T^R/F_T^V, and F_W^R/F_W^V (panel (a), (b), and (c), respectively) as a function of the dimensionless parameter G_c/h_w.

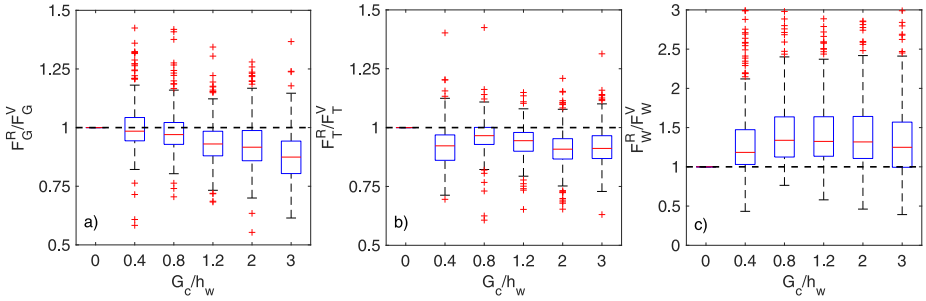

Fig. 8. Boxplot of the ratios F_G^R/F_G^V, F_T^R/F_T^V, and F_W^R/F_W^V (panel (a), (b), and (c), respectively) as a function of the dimensionless parameter G_c/h_w. Note: on each box, the central mark (red line) indicates the median, and the bottom and top edges of the box indicate the 25th and 75th percentiles, respectively. The whiskers extend to the most extreme data points not considered outliers, and the outliers are plotted individually using red cross markers.

25th, and 75th percentiles) have been calculated for each set of force components ratios and are presented and discussed in the following.

Fig. 7 represents with black empty markers the average value of the ratios F_G^R/F_G^V, F_T^R/F_T^V, and F_W^R/F_W^V (panels (a), (b), and (c), respectively) as a function of the dimensionless parameter G_c/h_w. Looking at the panel (a), it can be seen that F_G^R/F_G^V is, as expected, equal to 1 for $G_c/h_w = 0$ (flushed wall). For small values of G_c/h_w (i.e., small wall retreats) it is very close to, or even slightly larger than, 1. Conversely, for increasing values of G_c/h_w (i.e., larger wall retreats), this ratio tends to diminish, exhibiting a fairly linear trend, reaching a minimum value of 0.87 for the largest wall retreat tested (G_{c5}).

A similar behavior is observed for the ratio F_T^R/F_T^V (panel (b) of the same figure). In fact, this ratio (equal to 1 for $G_c/h_w = 0$) tends to decrease linearly in the range $0 \le G_c/h_w \le 1.2$, reaching a minimum value of 0.91, while tends to remain almost constant for increasing values of G_c/h_w, exhibiting an asymptotical behavior.

A completely different behavior is noticeable for the ratio F_W^R/F_W^V (panel (c) of the same figure). In this case, F_G^R/F_G^V (equal to 1 for $G_c/h_w = 0$) increases quickly for increasing values of G_c/h_w and attains at value of the order of 1.5. This suggests two considerations related to the forces acting on retreated wave walls: on the one hand it seems that exists a kind of "on–off" mechanisms of the force increase acting on retreated wave walls, while on the other hand it appears that exists a "saturation" of the force increase itself within the range of the tested wall retreats.

In order to provide with an idea of the dispersion of the data, Fig. 8 reports the boxplots as a function of G_c/h_w. On each box, the central mark (red line) indicates the median, and the bottom and top edges of the box indicate the 25th and 75th percentiles, respectively. The whiskers extend to the most extreme data points not considered outliers, and the outliers are plotted individually using red cross markers. Similarly to what done in Fig. 7, the panel (a) refers to the ratios F_G^R/F_G^V, the panel (b) to F_T^R/F_T^V, and the panel (c) to F_W^R/F_W^V, respectively. These representations, together with the statistical indicators reported in the Tables 3, 4, and 5, can be useful for preliminary design purposes as they give a direct measure of the variability, as well as of the uncertainty, related to such phenomena. In particular, the panel (c) shows that the highest variability and uncertainty, testified by the significant difference between the 25th and 75th percentiles, is related, as expected, to the forces acting on the wave wall.

Table 3
Statistical descriptors of the ratios F_G^R/F_G^V as a function of G_c/h_w.

G_c/h_w	Mean	Median	25th percentile	75th percentile
0.00	1.00	1.00	1.00	1.00
0.40	1.01	0.98	0.94	1.04
0.80	0.98	0.97	0.92	1.02
1.20	0.93	0.93	0.87	0.98
2.00	0.92	0.91	0.85	0.98
3.00	0.87	0.87	0.80	0.94

Table 4
Statistical descriptors of the ratios F_T^R/F_T^V as a function of G_c/h_w.

G_c/h_w	Mean	Median	25th percentile	75th percentile
0.00	1.00	1.00	1.00	1.00
0.40	0.96	0.92	0.86	0.96
0.80	0.93	0.96	0.92	1.00
1.20	0.91	0.94	0.89	0.97
2.00	0.91	0.90	0.86	0.95
3.00	0.92	0.91	0.86	0.96

Table 5
Statistical descriptors of the ratios F_W^R/F_W^V as a function of G_c/h_w.

G_c/h_w	Mean	Median	25th percentile	75th percentile
0.00	1.00	1.00	1.00	1.00
0.40	1.40	1.18	1.03	1.47
0.80	1.50	1.33	1.12	1.64
1.20	1.45	1.32	1.13	1.64
2.00	1.42	1.31	1.11	1.64
3.00	1.34	1.25	1.00	1.57

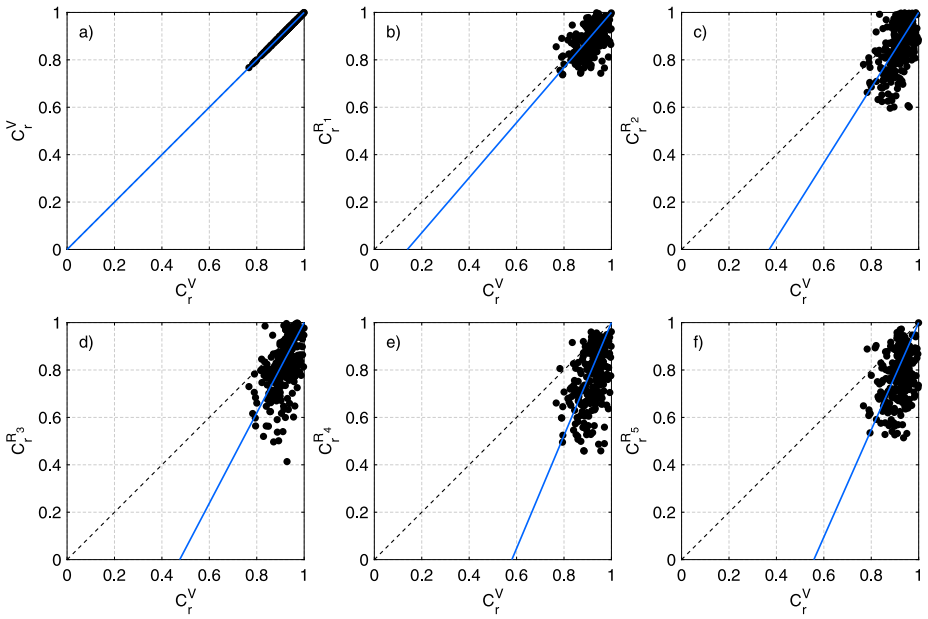

Fig. 9. Scatter plots of the reflection coefficients (filled black markers). In the panels from (b) (referring to G_{c1}) to (f) (referring to G_{c5}), $C_r^{R_i}$ are plotted against C_r^V, while in the panel (a) the same quantities (C_r^V, referring to G_{c0}) are reported in both the x- and y-axes. Note: the dashed black and continuous blue lines identify the bisector and trend lines, respectively.

3.2. Reflection coefficients

In this section the analysis of the reflection coefficients as a function of the wall position is presented and discussed. For each test, the incident and reflected wave components have been separated using the nonlinear method by Andersen et al. (2017), and the reflection coefficient (C_r) calculated as the ratio of the reflected and of the incoming wave height (referred to as H). The analysis has been carried out in the same time window considered for the evaluation of the forces, in which stationary conditions acting on the structure are guaranteed. In the following: C_r^V and $C_r^{R_i}$ refer respectively to the flushed wall configuration (G_{c0}) and to the five retreated wall configurations (G_{c1}–G_{c5}), as also reported in the List of Symbols.

The analysis of the reflection coefficients is presented in Fig. 9. Coherently with what done for the force analysis, the experimental data are represented as filled black markers and are presented in the form of scatter plots, while the dashed black and continuous blue lines identify the bisector and the best fitting lines, respectively. Note that the organization of this figure is exactly the same of Figs. 4, 5, and 6.

Panel (a) of Fig. 9 shows that, as obvious, the data lie exactly along the bisector line (G_{c0}). Conversely, a different behavior of the reflection coefficients is noticed for increasing retreats of the wave wall (G_{c1}–G_{c5}), represented in the panels from (b) to (f). For small wall retreats (panels (b) and (c)), the data cloud, although characterized by dispersion, tend to lie on the right of the bisector lines. This testifies that the reflection coefficients tends to decrease, on average, with increasing G_c. In fact, also for small wall retreats, the disturbances on the pulsating flow regime induced by the wall retreat changes the nature of the wave reflection increasing turbulent dissipation and resulting in a lower reflection coefficient. This behavior tends to be magnified as larger wall retreats are considered (panels (d), (e) and (f)). In fact, for larger wall retreats the data cloud tends to move, on average, even more on the right of the bisector lines, as clearly shown by the trend lines. Moreover, the vertical dispersion of the experimental data increases with G_c and the reflection coefficients exhibit minima values in the order of 0.5 for large G_c (see panels (d), (e) and (f)). This trend, already highlighted by Romano and Bellotti (2023), which analyzed a reduced number of wave and geometrical conditions, is confirmed by these new experiments.

Table 6
Statistical descriptors of the ratios C_r^R/C_r^V as a function of G_c/h_w.

G_c/h_w	Mean	Median	25th percentile	75th percentile
0.00	1.00	1.00	1.00	1.00
0.40	0.97	0.97	0.93	1.01
0.80	0.93	0.93	0.86	1.00
1.20	0.89	0.91	0.83	0.97
2.00	0.83	0.84	0.75	0.92
3.00	0.83	0.83	0.76	0.91

The ratios between the reflection coefficients measured for all the retreated wall configurations ($C_r^{R_i}$) and those for the flushed wall configuration (C_r^V), obtained for the same conditions, have then been calculated, along with some statistical parameters. Similarly to what done for the ratios of the forces, in panel (a) of Fig. 10 are reported as black empty markers the average values of the ratios C_r^R/C_r^V, while in panel (b) of the same figure, other statistical descriptors of the same ratios are represented in the form of boxplots as a function of G_c/h_w. Note that symbols and notation for the boxplots are the same as those used in Fig. 8.

Looking at the panel (a), it can be seen that for increasing values of G_c/h_w, C_r^R/C_r^V tends to decrease almost linearly up to $G_c/h_w = 2$, reaching the minimum value of 0.83. Instead, for $G_c/h_w > 2$, it appears that C_r^R/C_r^V tends to remain constant, without experiencing further increase nor reduction. So, it appears that, on average, also for the reflection coefficient, the reduction caused by the wall retreat seems to be limited and, at least for the considered range of parameters, does not further decrease beyond certain values of wall retreats. A similar behavior is confirmed looking at the boxplots represented in the panel (b) of Fig. 10. In fact, the medians of the C_r^R/C_r^V tends to decrease linearly up to $G_c/h_w = 2$ and then stabilize (see Table 6).

3.3. Wave overtopping

In this section the analysis of the average wave overtopping discharge q (l/m/s), as a function of the wall position, is presented and discussed. The overtopping waves have been collected in the tank located behind the wave wall and the total volume, recorded during

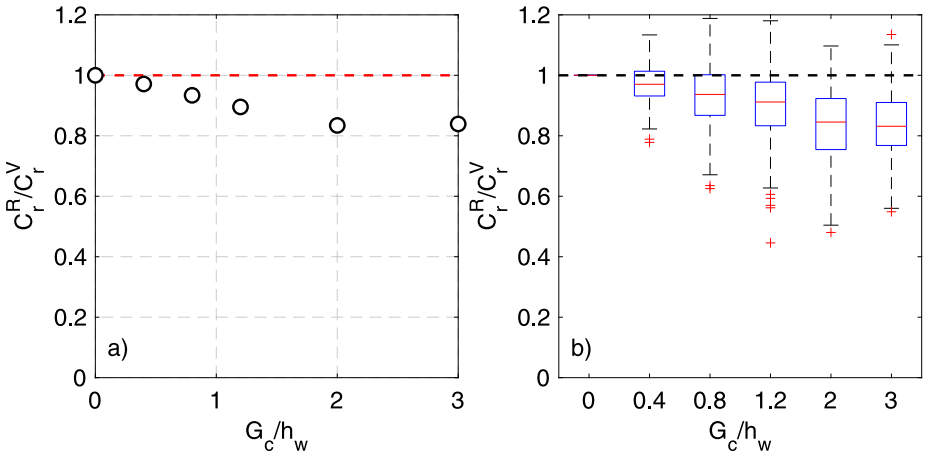

Fig. 10. Panel (a): average values (empty black markers) of the ratios C_r^R/C_r^V as a function of the dimensionless parameter G_c/h_w. Panel (b): boxplots of the ratios C_r^R/C_r^V as a function of the dimensionless parameter G_c/h_w. Note: on each box, the central mark (red line) indicates the median, and the bottom and top edges of the box indicate the 25th and 75th percentiles, respectively. The whiskers extend to the most extreme data points not considered outliers, and the outliers are plotted individually using red cross markers.

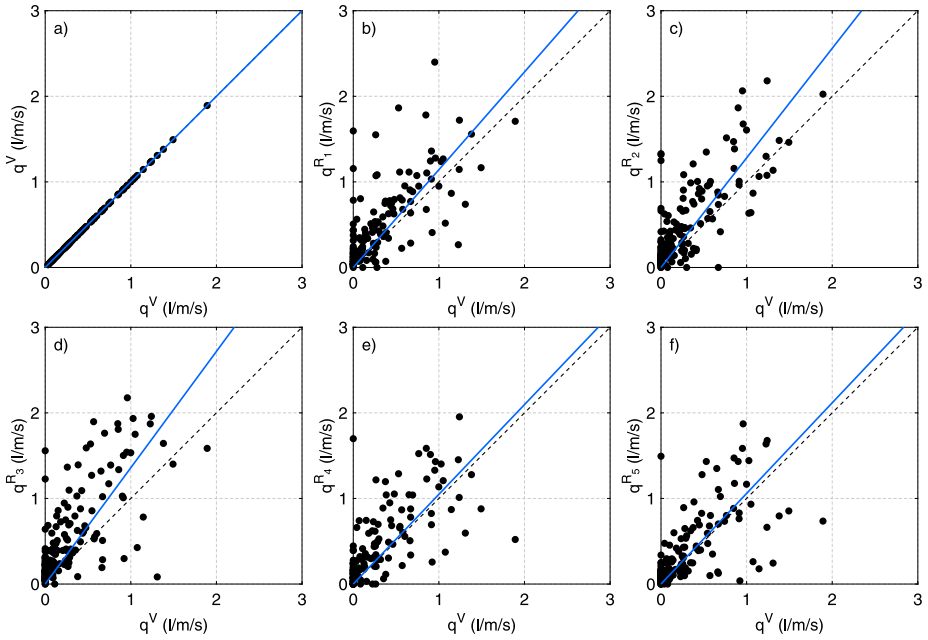

Fig. 11. Scatter plots of the wave overtopping discharges (filled black markers). In the panels from (b) (referring to G_{c1}) to (f) (referring to G_{c5}), q^{R_i} are plotted against q^V, while in the panel (a) the same quantities (q^V, referring to G_{c0}) are reported in both the x- and y-axes. Note: the dashed black and continuous blue lines identify the bisector and trend lines, respectively.

the same time window used for both the forces and reflection analysis, has been evaluated on the basis of the measurement of the free surface elevation in the tank. The volume has been then divided by the width of the overtopping chute and by the time duration of the considered time window. Finally, the average overtopping discharge q is available for each experimental test.

Given that regular waves are used and that the analysis is carried out on short time windows, an important clarification on the meaning of q is needed. In fact, these values of q cannot be intended in a "classical sense" as the average overtopping discharge that can be calculated by using literature formulae (EurOtop, 2018). Indeed, it is well known that wave overtopping is a complex phenomenon and the mean overtopping discharge is an hydraulic parameter that is normally evaluated under the attack of random (irregular) sea states and closely depends on the test duration, on the number of reproduced waves, on the wave sequencing, and on other aspects not considered here (Romano et al., 2015; Williams et al., 2019). On the contrary, these values of q should be considered as a mean to compare some structural layouts, similarly to what done by Castellino et al. (2018, 2021). The aim of this analysis is, in fact, to compare the wave overtopping performances of a structure with retreated wave wall with those of the same structure with flushed wall under the same wave conditions. The analysis is expected to provide a measure of the increase/reduction factor of wave overtopping induced by a retreated wave wall or, in other words, the deviation from the flushed wall behavior.

The following symbols are used throughout the paper: q^V and q^{R_i}, respectively the wave overtopping discharge for the flushed wall configuration (G_{c0}) and the same quantity related to the five retreated wall configurations (G_{c1}–G_{c5}). The analysis of the wave overtopping is presented in Fig. 11; it is organized exactly as the Figs. 4, 5, 6, and 9. In general, the wave overtopping discharge increases for increasing values of G_c, as clearly shown by the trend lines. This aspect, which is completely new as the wave overtopping was not measured by Romano and Bellotti (2023), is somehow expected. In fact, the change of flow regime induced by the wall retreat, modifies the nature of the wave-structure interaction hydrodynamics. A bore, with significant

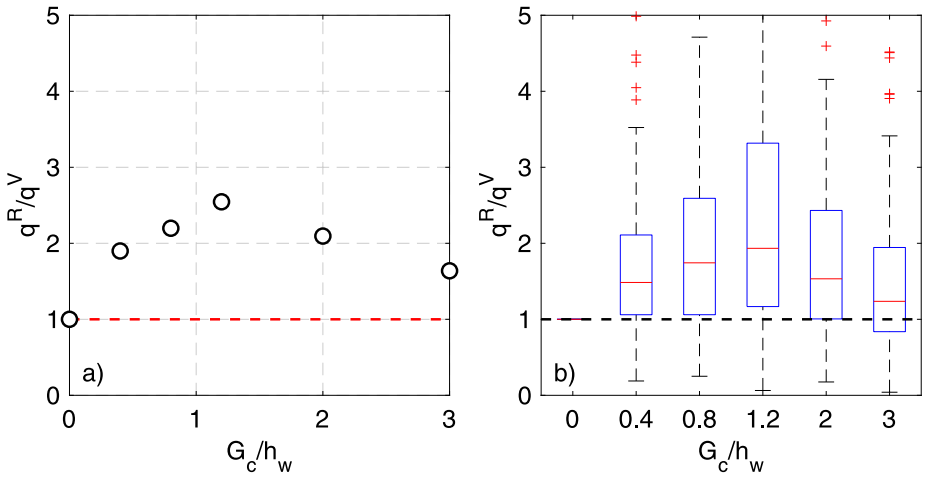

Fig. 12. Panel (a): average values (empty black markers) of the ratios q^R/q^V as a function of the dimensionless parameter G_c/h_w. Panel (b): boxplots of the ratios q^R/q^V as a function of the dimensionless parameter G_c/h_w. Note: on each box, the central mark (red line) indicates the median, and the bottom and top edges of the box indicate the 25th and 75th percentiles, respectively. The whiskers extend to the most extreme data points not considered outliers, and the outliers are plotted individually using red cross markers.

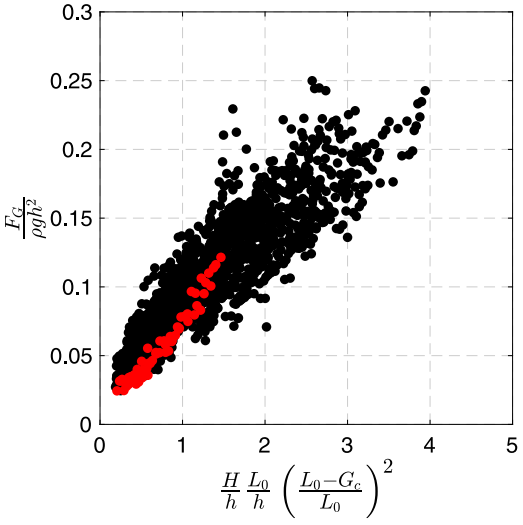

Fig. 13. Dimensionless global $\frac{F_G}{\rho g h^2}$ forces obtained in all the experimental tests and for all the wall configurations as a function of the explanatory variable $\frac{H}{h}\frac{L_0}{h}\left(\frac{L_0-G_c}{L_0}\right)^2$. Note: filled red and black circles represent data of Romano and Bellotti (2023) and new small-scale data, respectively.

horizontal momentum, develops on the flat superstructure between the seaward edge of the trunk and the wave wall: after impacting the wall, it seems to favor the occurrence of overtopping. This is particularly evident, especially for those "on the edge conditions", in which null or little wave overtopping would have been occurred if a flushed wall configuration would have been used.

Furthermore, looking at Fig. 11, it is possible to see that the dispersion of experimental data is relevant, as expected for a complex phenomenon like the wave overtopping, characterized by large sources of uncertainties (Romano et al., 2015; Williams et al., 2019), even if regular waves are used. For small and medium wall retreats (panels (b), (c) and (d)), the data cloud, although characterized by dispersion, shows that the wave overtopping discharge tends to increase significantly with respect to the flushed wall configuration. In fact, for small and medium wall retreats, the data cloud tends to move, on average, significantly on the left of the bisector lines, as clearly shown by the trend lines. On the contrary, this behavior tends to be less evident as far as larger wall retreats are considered (panels (e) and (f)), where,

Table 7
Statistical descriptors of the ratios q^R/q^V as a function of G_c/h_w.

G_c/h_w	Mean	Median	25th percentile	75th percentile
0.00	1.00	1.00	1.00	1.00
0.40	1.90	1.48	1.06	2.11
0.80	2.20	1.74	1.06	2.59
1.20	2.55	1.93	1.16	3.31
2.00	2.01	1.53	1.00	2.43
3.00	1.63	1.23	0.84	1.95

although the data dispersion is even more pronounced, the rate of wave overtopping increase tends to decrease.

Similarly to what already discussed with reference to the reflection coefficient ratios (Fig. 10), in panel (a) of Fig. 12 the mean values of the ratios q^R/q^V are represented with black empty markers, while in panel (b) of the same figure, other statistical descriptors of the same quantity are reported using boxplots. The notation is identical to that used for the other parameters. The ratio q^R/q^V increases quickly with G_c/h_w, almost linearly, and reaches a maximum value of 2.55 for $G_c/h_w = 2$. Then, it starts to decrease, with a linear trend characterized by a slope less pronounced than that of the ascending phase, reaching a minimum value of 1.63 for $G_c/h_w = 3$ (i.e., G_{c5}, the largest wall retreat tested during the experiment). A similar behavior is confirmed by the boxplots represented in the panel (b) of Fig. 12. It is worth noticing that the boxplots are particularly useful to represent the large variability/uncertainty that characterizes the wave overtopping. In fact, it is possible to see that experimental data present a large gap between 25th and 75th percentiles, especially for the largest values of wave overtopping increase (see Table 7). In general, it appears that there exist some wall positions, for which the maximum values of overtopping increase.

3.4. Limitations

In this section, the limitations of the present study, as well as the coherence with previous findings, are discussed. The most important limitation is related to the chosen reduction scale factor, that is in the order of 1:100, if reference is made to the typical dimension of vertical breakwaters. The reason of such a choice is the following. The experimental evidences described by Romano and Bellotti (2023), highlighted the complex nature of the processes induced by a retreated wall, which changes dramatically the hydrodynamics of the

wave-structure interaction, governed by the complex mutual interaction between several (often antithetical) factors/drivers. Those factors have been clearly identified in the previous research, but a very limited number of combinations of the geometry and of the wave parameters had been tested. The complexity of the phenomenon at hand, together with its high degree of variability/uncertainty, has led the Authors to prefer a large number of experiments in a small wave flume instead of a smaller number of tests in a larger facility, like that adopted in the previous campaign. This choice is often preferred to understand complex physical processes of wave-structure interaction (Ravindar et al., 2021). In fact, the small experimental setup, which is similar to that used by Romano et al. (2015), has guaranteed a high degree of flexibility, a short duration of each experiment and, accordingly, a short time lag between two consecutive experiments.

The results are therefore certainly affected by some scale effects. However, it should be noted that the aim of this study is not to provide absolute values of forces, reflection coefficients, overtopping discharges, nor design empirical formulae. Instead, the aim of this campaign is to provide some comparison, in terms of the ratio of hydraulic parameters, of the performances (force, reflection coefficients, wave overtopping) of a structure with retreated wave wall against those of the same structure with flushed wall under the same wave conditions. Both the configurations (flushed and retreated), are expected to experience similar laboratory and scale effects. Obviously, some processes (e.g., presence of air bubbles, air entrainment in the bore, water compressibility) are more affected than others if a reduced scale is used (Bullock et al., 2001; Blenkinsopp and Chaplin, 2011; Ravindar et al., 2021), but the general trend/behavior, especially if intended in a comparative way, should be well caught. In fact, the new experimental results confirm and extend the understanding of the complex physical mechanisms as well as the results and findings pointed out by Romano and Bellotti (2023) at a larger scale.

In this regard, reference can be made to Fig. 13. It is identical to Figure 19 of Romano and Bellotti (2023), and reports the dimensionless global $\frac{F_G}{\rho g h^2}$ forces, obtained for all the experimental tests and for all the wall configurations, as a function of the explanatory variable $\frac{H}{h}\frac{L_0}{h}\left(\frac{L_0-G_c}{L_0}\right)^2$, proposed by Romano and Bellotti (2023). Note that filled red and black circles represent data of Romano and Bellotti (2023) and new small-scale data, respectively. This figure shows that the experimental data obtained at a larger scale, fall within the cloud formed by the new small-scale experiments. Moreover, the wide expansion of the experimental ranges of the tested parameters and the complexity of the hydrodynamics phenomena at hand, reflected in the significant dispersion of the experimental data, suggested to adopt a statistical approach, based on a large number of experimental tests, instead of trying to provide explanatory variables and empirical formulae (e.g., Figures 21 and 22 of Romano and Bellotti, 2023).

Another limitation lies in using regular, instead of irregular, waves in the tests. The reasons for this choice is, again, that of reducing the duration of each run, in order to carry out a very large number of tests, and of avoiding the uncertainty in the results interpretation induced by the randomness of a real sea state. The results cannot therefore be used directly for estimating the effects of real sea states on the structures. However, they can surely be used to compare the performances of the breakwaters under the action of identical wave conditions, though regular. A similar approach has been recently used with success by Martinelli et al. (2018) and Castellino et al. (2021). They have demonstrated that the effect, in terms of maximum forces induced by an irregular sea state acting on a vertical breakwater, can be well reproduced using regular waves. Certainly, the wave overtopping is expected to be much more influenced by the randomness and by the sequence of the waves and further research is deemed necessary, to better investigate this important hydraulic performance parameter.

Finally, two further possible scale and laboratory effects should be considered: (1) the use of relatively rough elements in small scales, that can affect the porosity and roughness of the mound, resulting in some critical effects on the rock stability, that however are not considered in the paper; (2) the occurrence of sub-harmonic long waves, typical of any wave flume experiments, that can induce local set-ups/downs at the structure. In this case, the short duration of the experiments is expected to limit their occurrence. Therefore, it is noted that neither of the aforementioned is expected to have a significant impact on the experimental results.

4. Conclusions

In this paper, the results of a new small-scale experimental campaign aiming at investigating the hydraulic performances (forces, reflection coefficients and wave overtopping) of composite vertical breakwaters with retreated wave wall have been presented. This new campaign represents a wide expansion of the previous work of Romano and Bellotti (2023), that investigated the basic phenomena involved and the related governing factors.

Due to the complex nature of the hydrodynamic processes at hand, which is governed by the mutual interaction between the governing drivers, in this new campaign it was chosen to explore and vary systematically both wave and geometrical parameters, performing a very large number of small-scale tests (in the order of 2,000) with regular waves. On the basis of the large number of experimental data, a robust statistical analysis has been performed, to provide a quantitative estimate of the force, reflection coefficient, and wave overtopping increase/reduction factor, compared to the flushed wall configuration, as a function of the wall retreat. These results can be used as first guidelines for engineering design of such structures.

As a general result, the experimental evidences confirm and extend the understanding of the physical processes as well as the previous findings pointed out by Romano and Bellotti (2023). Specifically, the forces acting on the wave wall are, on average, 1.5 times larger than those occurring on a flushed wall configuration under the same wave conditions. This increase, which seems to be characterized by an "on-off" mechanisms, is due to the occurrence of impulsive loads conditions, which occur for all the wall retreat configurations, and tends to remain almost constant also for large wall retreats. The forces acting on the caisson trunk, on average, tend to decrease with increasing G_c, reaching a minimum average reduction factor of 0.91. Also for the trunk forces, the reduction factor remains almost constant for $G_c/h_w > 1.2$. As far as global forces are concerned, it appears that, on average, they decrease with increasing G_c, reaching a minimum reduction factor, compared with flushed wall configurations, of 0.87. Moreover, it is worth noticing that this general behavior of the global forces presents some dangerous exceptions, in which equal or larger loads, than those occurring for standard flushed wall configuration, are experienced by the structure in the range $0 \le G_c/h_w \le 1$. This was already highlighted by Romano and Bellotti (2023) and appears to be due to the complex (often antithetical) interaction between the governing drivers/factors (impulsive impacts on wall, trunk-wall loads time shifting, reduction of pressures at the seaside edge of the trunk), and is particularly critical for the stability of these structures.

As far as reflection coefficients are concerned, the experimental data suggest that this parameter, on average, decreases with increasing values of G_c, reaching a minimum reduction factor of 0.83. Similarly to what seen for trunk forces, this reduction factor tends to remain constant, without experiencing further increase nor reduction beyond certain values of wall retreats.

Moreover, the wave overtopping performances have been investigated. This aspect is completely new as not considered in the previous paper of Romano and Bellotti (2023). As a general result, the experimental evidences, although characterized by large variability, suggested that a structure with retreated wall experiences wave overtopping discharges larger than those occurring for flushed wall configurations under the same wave conditions. This is particularly evident,

especially for those "on the edge conditions", in which null or little wave overtopping would have been occurred for the flushed wall configuration. Specifically, the wave overtopping increase factor reaches, on average, a maximum value of 2.55 for $G_c/h_w = 2$, while decreasing up to a minimum value of 1.63 for $G_c/h_w = 3$ (i.e., G_{c5}, the largest wall retreat tested during the experiment).

To summarize, both the previous (Romano and Bellotti, 2023) and the new experimental results suggest that the wave-structure interaction phenomena that take place at structures with retreated wave wall are quite complicated. For this reason, a note of extra caution should be adopted when designing these structures. In fact, this paper provides statistical indicators which can be used as guidelines for preliminary design purposes, nevertheless it is recommended to plan an ad-hoc physical/numerical tests campaign tailored on the specific case.

Finally, it is worth to stress that, due to the complexity of the phenomena that take place, further research would be valuable. Specifically, it would be useful to explore the possibility of using Machine Learning techniques to develop predictive tools. At the same time, a careful analysis and classification, using hybrid modeling techniques and computational fluid dynamics (CFD) methods, of the bores propagating on the promenade and impacting the wave wall would allow to identify those hydrodynamic conditions that represent the "the worst-case scenario" for the structure. Finally, it would be worth to study the effect of irregular (random) wave conditions for refining the quantification of wave overtopping uncertainty.

List of symbols

- C_r^V = reflection coefficient related to the flushed wall configuration, (–);
- $C_r^{R_i}$ = reflection coefficient related to the ith ($i = 1, \ldots, 5$) retreated wall configuration, (–);
- C_r^R/C_r^V = average values of the ratios $C_r^{R_i}/C_r^V$, (–);
- $F_G(t)$, $F_T(t)$, $F_W(t)$ = global, trunk and wall force time series, (N/m);
- F_G, F_T, F_W = average values of global, trunk and wall force peaks, (N/m);
- F_G^V, F_T^V, F_W^V = average values of global, trunk and wall force peaks related to the flushed wall configuration, (N/m);
- $F_G^{R_i}$, $F_T^{R_i}$, $F_W^{R_i}$ = average values of global, trunk and wall force peaks related to the ith ($i = 1, \ldots, 5$) retreated wall configuration, (N/m);
- F_G^R/F_G^V, F_T^R/F_T^V, F_W^R/F_W^V = average values of the ratios $F_G^{R_i}/F_G^V$, $F_T^{R_i}/F_T^V$, $F_W^{R_i}/F_W^V$, (–);
- g = gravitational acceleration, (m/s^2)
- G_c = wave wall retreat, (m)
- $G_{c0} = G_c$ of the flushed wall configuration ($G_c = 0.0$ m), (m)
- G_{c1}–$G_{c5} = G_c$ of the five retreated wall configurations, (m)
- h = water depth, (m)
- h_b = rubble mound foundation height, (m)
- h_t = caisson trunk height, (m)
- h_w = wave wall height, (m)
- H = incident wave height, (m)
- L_0 = deep-water wavelength, (m)
- q^V = wave overtopping discharge related to the flushed wall configuration, (l/m/s);
- q^{R_i} = wave overtopping discharge related to the ith ($i = 1, \ldots, 5$) retreated wall configuration, (l/m/s);
- q^R/q^V = average values of the ratios q^{R_i}/q^V, (–);
- R_c = crest freeboard, (m)
- T = wave period, (s)
- ρ = water density, (kg/m^3)

CRediT authorship contribution statement

Alessandro Romano: Writing – review & editing, Writing – original draft, Visualization, Methodology, Investigation, Formal analysis, Data curation, Conceptualization. **Matteo Centorami:** Writing – review & editing, Writing – original draft, Investigation, Formal analysis, Data curation. **Claudia Cecioni:** Writing – review & editing, Writing – original draft, Methodology, Investigation, Conceptualization. **Giorgio Bellotti:** Writing – original draft, Methodology, Investigation, Funding acquisition, Conceptualization.

Declaration of competing interest

The authors declare that they have no known competing financial interests or personal relationships that could have appeared to influence the work reported in this paper.

Data availability

Data will be made available on request.

Acknowledgments

A special acknowledgment is due to Rachele Proietti Tocca, for participating to the experimental campaign, and to Prof. Aldo Fiori for the useful discussions on the statistical analyses.

References

Aalborg University, A., 2018. Awasys 7. [www document]. URL www.hydrosoft.civil.aau.dk/awasys.

Andersen, T.L., Clavero, M., Eldrup, M.R., Frigaard, P.B., Losada, M., 2018. Active absorption of nonlinear irregular waves. In: Coastal Engineering 2018. Coastal Engineering Research Council.

Andersen, T.L., Clavero, M., Frigaard, P., Losada, M., Puyol, J., 2016. A new active absorption system and its performance to linear and non-linear waves. Coast. Eng. 114, 47–60.

Andersen, T.L., Eldrup, M.R., Frigaard, P., 2017. Estimation of incident and reflected components in highly nonlinear regular waves. Coast. Eng. 119, 51–64.

Blenkinsopp, C., Chaplin, J., 2011. Void fraction measurements and scale effects in breaking waves in freshwater and seawater. Coast. Eng. 58, 417–428.

Bredmose, H., Bullock, G., Hogg, A., 2015. Violent breaking wave impacts. part 3. effects of scale and aeration. J. Fluid Mech. 765, 82–113.

Bredmose, H., Peregrine, D., Bullock, G., 2009. Violent breaking wave impacts. part 2: modelling the effect of air. J. Fluid Mech. 641, 389–430.

Bullock, G., Crawford, A., Hewson, P., Walkden, M., Bird, P., 2001. The influence of air and scale on wave impact pressures. Coast. Eng. 42, 291–312.

Bullock, G., Obhrai, C., Peregrine, D., Bredmose, H., 2007. Violent breaking wave impacts. part 1: Results from large-scale regular wave tests on vertical and sloping walls. Coast. Eng. 54, 602–617.

Cao, D., Yuan, J., Chen, H., Zhao, K., Liu, P.L.F., 2021. Wave overtopping flow striking a human body on the crest of an impermeable sloped seawall. part i: Physical modeling. Coast. Eng. 167, 103891.

Castellino, M., Romano, A., Lara, J.L., Losada, I.J., De Girolamo, P., 2021. Confined-crest impact: Forces dimensional analysis and extension of the goda's formulae to recurved parapets. Coast. Eng. 163, 103814.

Castellino, M., Sammarco, P., Romano, A., Martinelli, L., Ruol, P., Franco, L., De Girolamo, P., 2018. Large impulsive forces on recurved parapets under non-breaking waves. a numerical study. Coast. Eng. 136, 1–15.

Chen, X., Hofland, B., Altomare, C., Suzuki, T., Uijttewaal, W., 2015. Forces on a vertical wall on a dike crest due to overtopping flow. Coast. Eng. 95, 94–104.

Chen, H., Yuan, J., Cao, D., Liu, P.L.F., 2021. Wave overtopping flow striking a human body on the crest of an impermeable sloped seawall. part ii: Numerical modelling. Coast. Eng. 168, 103892.

Cooker, M., Peregrine, D., 1990. Computations of violent motion due to waves breaking against a wall. In: Proc. 22nd Intl. Conf. on Coastal Engineering. ASCE, pp. 164–176.

Cuomo, G., Allsop, W., Bruce, T., Pearson, J., 2010a. Breaking wave loads at vertical seawalls and breakwaters. Coast. Eng. 57, 424–439.

Cuomo, G., Allsop, W., Takahashi, S., 2010b. Scaling wave impact pressures on vertical walls. Coast. Eng. 57, 604–609.

De Finis, S., Romano, A., Bellotti, G., 2020. Numerical and laboratory analysis of post-overtopping wave impacts on a storm wall for a dike-promenade structure. Coast. Eng. 155, 103598.

De Rouck, J., Van Doorslaer, K., Versluys, T., Ramachandran, K., Schimmels, S., Kudella, M., Trouw, K., 2012. Full scale impact tests of an overtopping bore on a vertical wall in the large wave flume (gwk) in hannover. Coast. Eng. Proc. 1, 33.

EurOtop, 2018. In: van der Meer, J.W., Allsop, N.W.H., Bruce, T., J.J., De Rouck, Kortenhaus, A., Pullen, T., Schüttrumpf, H., Troch, P., Zanuttigh, B. (Eds.), Manual on Wave Overtopping of Sea Defences and Related Structures. www.overtopping-manual.com.

Franco, L., 1994. Vertical breakwaters: the italian experience. Coast. Eng. 22, 31–55.

Goda, Y., 2010. Random Seas and Design of Maritime Structures, vol. 33, World Scientific Publishing Company.

Martin, F.L., Losada, M.A., Medina, R., 1999. Wave loads on rubble mound breakwater crown walls. Coast. Eng. 37, 149–174.

Martinelli, L., Lamberti, A., 2011. Dynamic response of caisson breakwaters: suggestions for the equivalent static analysis of a single caisson in the array. Coast. Eng. J. 53, 1–20.

Martinelli, L., Ruol, P., Volpato, M., Favaretto, C., Castellino, M., De Girolamo, P., Franco, L., Romano, A., Sammarco, P., 2018. Experimental investigation on non-breaking wave forces and overtopping at the recurved parapets of vertical breakwaters. Coast. Eng. 141, 52–67.

Molines, J., Bayon, A., Gómez-Martín, M.E., Medina, J.R., 2019. Influence of parapets on wave overtopping on mound breakwaters with crown walls. Sustainability 11, 7109.

Oumeraci, H., Kortenhaus, A., Allsop, W., de Groot, M., Crouch, R., Vrijling, H., Voortman, H., 2001. Probabilistic Design Tools for Vertical Breakwaters. CRC Press.

Ravindar, R., Sriram, V., Schimmels, S., Stagonas, D., 2021. Approaches in scaling small-scale experiments on the breaking wave interactions with a vertical wall attached with recurved parapets. J. Waterw. Port Coast. Ocean Eng. 147, 04021034.

Romano, A., Bellotti, G., 2023. Wave forces on vertical caissons with retreated wall: A first experimental insight. Coast. Eng. 186, 104396.

Romano, A., Bellotti, G., Briganti, R., Franco, L., 2015. Uncertainties in the physical modelling of the wave overtopping over a rubble mound breakwater: The role of the seeding number and of the test duration. Coast. Eng. 103, 15–21.

Takahashi, S., 1996. Design of vertical breakwaters. breakwater design. In: International Conference on Coastal Engineering. Orlando, Short Course.

Van Doorslaer, K., Romano, A., De Rouck, J., Kortenhaus, A., 2017. Impacts on a storm wall caused by non-breaking waves overtopping a smooth dike slope. Coast. Eng. 120, 93–111.

van Gent, M.R., 2003. Wave overtopping events at dikes. In: Coastal Engineering 2002: Solving Coastal Conundrums. World Scientific, pp. 2203–2215.

Williams, H.E., Briganti, R., Romano, A., Dodd, N., 2019. Experimental analysis of wave overtopping: A new small scale laboratory dataset for the assessment of uncertainty for smooth sloped and vertical coastal structures. J. Mar. Sci. Eng. 7 (217).